Hindawi Publishing Corporation
Physics Research International
Volume 2012, Article ID 576547, 14 pages
doi:10.1155/2012/576547

Review Article

Second-Order Nonlinear Optical Microscopy of a H–Si(111)1 × 1 Surface in Ultra-High Vacuum Conditions

Yoshihiro Miyauchi[1,2]

[1] *School of Materials Science, Japan Advanced Institute of Science and Technology, 1-1 Asahidai, Nomi, Ishikawa 923-1292, Japan*
[2] *Core Research for Evolutional Science and Technology, Japan Science and Technology Corporation, 5-3 Yonbancho, Chiyoda-ku, Tokyo 102-8666, Japan*

Correspondence should be addressed to Yoshihiro Miyauchi, y-miyau@jaist.ac.jp

Received 2 December 2011; Accepted 10 February 2012

Academic Editor: Vladimir I. Gavrilenko

This paper reviews the use of optical sum frequency generation (SFG) and second harmonic generation (SHG) microscopy under ultra-high vacuum (UHV) conditions to observe the dynamics of a hydrogen terminated Si(111)1 × 1 surface. First, we took SFG and SHG microscopic images of the surface after IR light pulse irradiation and found that the SHG and nonresonant SFG signals were enhanced, probably due to the formation of dangling bonds after hydrogen desorption. Second, we observed time-resolved SFG intensity images of a H–Si(111)1 × 1 surface. After visible pump light irradiation, the nonresonant SFG signal increased at probe delay time 0 ps and then decreased over a life time of 565 ps. The resonant SFG signal reduced dramatically at 0 ps and then recovered with an anisotropic line shape over a life time of 305 ps. The areas of modulated SFG signals at delay time 277 ps were expanded with an anisotropic aspect. Finally, we observed SFG intensity images of hydrogen deficiency on a Si(111)1 × 1 surface as a function of temperature. These images of the H–Si(111) surface, taken with a spatial resolution of 5 μm at several temperatures from 572 to 744 K, showed that the hydrogen desorbs homogeneously.

1. Introduction

Most electronic devices are based on silicon technology. For example, the key process in a field-effect transistor (FET) is a gate stack on a Si surface [1]. The native oxide SiO_2 grown on the surface is a smooth layer having a dielectric free of trapped charge and defects; III–V compounds do not have such a suitable native oxide [1]. This is one of the reasons why silicon is the material of choice. Another advantage of silicon is that high-quality amorphous Si thin film can be grown on a Si surface using a chemical vapor deposition (CVD) process [2].

Hydrogen termination on a Si(H–Si) surface before the CVD process is a commonly used chemical treatment to protect the surface from oxidization. In the CVD process, the qualities of the thin layer depend on not only the radical reaction in the vapor phase but also an early reaction on the Si surface; hydrogen desorption is the central rule in that reaction [3]. Thus, for a decade, the structure and the dynamics on a H–Si surface were intensively studied using several methods, for example, FT-IR [4], STM [5, 6] HREELS [7], SHG [8], and SFG [9, 10]. However, some questions still remain unanswered. For example, the structure of a H–Si(111)1 × 1 surface studied by FT-IR [4] is inconsistent with that studied by reflection high-energy positron diffraction (RHEPD) [11]. In the FT-IR spectrum of a H–Si(111)1 × 1 surface chemical treated by dipping in an NH_4F solution, there is only one peak at 2083.7 cm^{-1} assigned to be the stretching mode of the monohydride [4]. However, from the results of RHEPD rocking curves, Kawasuso et al. concluded the surface prepared by a NH_4F solution is mostly terminated with monohydrides but trihydrides remain. They also suggest that there is roughness resulting from irregularly hydrogen-terminated parts, including trihydrides [11]. In order to resolve this inconsistency, it is necessary to observe the irregular parts with surface sensitive vibrational microscopy.

Another problem is that few studies have addressed the hydrogen dynamics on the surface when it is irradiated by a laser light pulse with high fluence and a pulse duration of

10 ps∼10 μs, even though this is an important process in the laser CVD method [12]. Spatial distribution of the hydrogen atoms with the scale of pulse spot size is especially crucial for quality of the deposited film.

In order to resolve these problems, surface-sensitive microscopy is necessary for observing the morphology of hydrogen species. However, few of the conventional methods are effective. A scanning tunneling microscope (STM) can show the spatial distribution of hydrogen molecules, but it is difficult to distinguish between the species. One the other hand, a scanning type microscope using electron-stimulated desorption (ESD) can also show the spatial distribution of hydrogen atoms [13]. With this method, hydrogen atoms on a Si surface are desorbed by ESD; they can then be detected by a time of flight technique. Using this method, a clear lithographed pattern of hydrogen on a Si surface was observed. However, it is not only a destructive method but it is also difficult to analyze the species. Conventional vibrational microscopy such as IR and Raman also lack surface sensitivity. Thus, a new method for observing the spatial distribution of hydrogen molecules on a Si surface has to be established.

In this paper, I review the application of sum frequency generation (SFG) and second harmonic generation (SHG) microscopy to the observation of the dynamics of hydrogen on a H–Si(111)1 × 1 surface. Especially, I demonstrate that new vibrational microscopy based on SFG microscopy is a useful tool for observing the morphology of hydrogen species. The paper is organized as follows. Section 2 briefly outlines the history and principles of nonlinear microscopy. Section 3 describes the experimental setup and sample preparation. Section 4 presents SFG and SHG intensity images of hydrogen deficiency on the Si surface after laser pulse irradiation. Section 5 introduces time-resolved (tr-) SFG microscopy of the surface. Section 6 shows the application of SFG microscopy for probing hydrogen diffusion. Finally, Section 7 summarizes the demonstrations of SFG and SHG microscopy.

2. SFG and SHG Microscopy

SFG and SHG are the lowest-order nonlinear optical processes. They occur in media without inversion symmetry and have high surface sensitivity [14]. SHG has been used as a tool to investigate the surface structures [15] and surface electronic states associated with dangling bonds on a Si surface [16, 17]. It was also used to estimate the speed of hydrogen adsorption [8] and the diffusion constant of hydrogen [18] on a Si(111) surface. In addition, it has been applied to probe charge trapping kinetics in thin films on Si surfaces [19] and the electronic states of Si nanocrystals [20]. Recently, the absolute phase and amplitude of a surface dipole at Si(001) interfaces was determined [21]. It has been applied to microscopy [22] for monitoring the spatial distribution of dangling bonds on a Si(111) surface by our group [23, 24].

SFG is a well-established tool for studying Si–H bonds [25] and identifying hydride species [9] on a Si surface. In 1999, Flörsheimer et al. demonstrated the first SFG microscopy, observing a Langmuir-Blodget thin film [26]. In 2007, Cimatu et al. observed SFG intensity images, distinguishing between self-assembled monolayers with different chain lengths in microprinted patterns [27]. However, no one has developed SFG microscopy for observing a sample in UHV conditions. Thus, we decided to develop a multifunctional SFG microscope to facilitate convenient analysis of a semiconductor surface under UHV conditions [28–32].

The output SFG signal with frequency $\omega = \omega_1 + \omega_2$ from a Si surface is given by [33]

$$S(\omega) \propto \left| \left[\overleftrightarrow{L}(\omega) \cdot \hat{e}(\omega) \right] \cdot \overleftrightarrow{\chi}_s^{(2)} : \left[\overleftrightarrow{L}(\omega_1) \cdot \hat{e}(\omega_1) \right] \times \left[\overleftrightarrow{L}(\omega_2) \cdot \hat{e}(\omega_2) \right] \right|^2 I_1 I_2 A T, \quad (1)$$

where $\overleftrightarrow{\chi}_s^{(2)}$, $\overleftrightarrow{L}(\omega_i)$, $\hat{e}(\omega_i)$, I_i, A, and T are surface nonlinear susceptibility, transmission Fresnel factor, polarization unit vector, intensity of the beam with frequency ω, the overlapping cross-section on the sample, and input pulse width, respectively. The bulk second-order nonlinear susceptibility is negligible due to the inversion symmetry of the Si crystal. In the case of $\omega_1 = \omega_2$, (1) represents the output SHG signal. In the following description of vibrational SFG, we assume visible light at ω_{vis} and IR light at ω_{IR} as the incident beams. With near vibrational resonances, $\overleftrightarrow{\chi}_s^{(2)}$ can be described as

$$\overleftrightarrow{\chi}_s^{(2)} = \overleftrightarrow{\chi}_{\text{NR}}^{(2)} + \sum_q \frac{\overleftrightarrow{A}_q}{\omega_{\text{IR}} - \omega_q + i\Gamma_q}, \quad (2)$$

where $\overleftrightarrow{\chi}_{\text{NR}}^{(2)}$ and $\overleftrightarrow{A}_q$, ω_{IR} and Γ_q are the nonresonant nonlinear susceptibility, and the strength, resonant frequency, and damping constant of the resonant mode, respectively [33]. When an infrared photon with energy $\hbar\omega_{\text{IR}}$ is scanned near the vibrational resonance of a molecule, the SFG intensity is enhanced, thus facilitating vibrational spectroscopy. Thus, in the images of the SFG light from a sample, we can distinguish between hydrogen species.

3. Experimental

The system for observing simultaneous SFG and SHG intensity images under UHV conditions is shown in Figure 1. In this SFG microcopy system, we used doubled frequency output from a mode-locked Nd^{3+} : YAG laser as the visible light at wavelength 532 nm, and output (∼4.8 μm) from an optical parametric generator and amplifier system (OPG/OPA) as the wavelength-tunable infrared light (IR probe light). The spectral bandwidth of the IR probe light was 6 cm^{-1}. The pulse energies of the IR probe and visible light beams were ∼100 μJ/pulse and ∼25 μJ/pulse, respectively.

The incident visible light was passed through a $\lambda/2$ plate, a Glan polarizer, a bandpass filter with a center wavelength of 532 nm, a lens with focal length $f = 300$ mm, and the CaF_2 window of the UHV chamber. The IR probe light was focused by a CaF_2 lens with a focal length of 300 mm. The angles of the incident visible and IR probe light beams were ∼45° and ∼60°, respectively.

The SFG light from the sample in the reflective direction was first passed through the glass window of the chamber

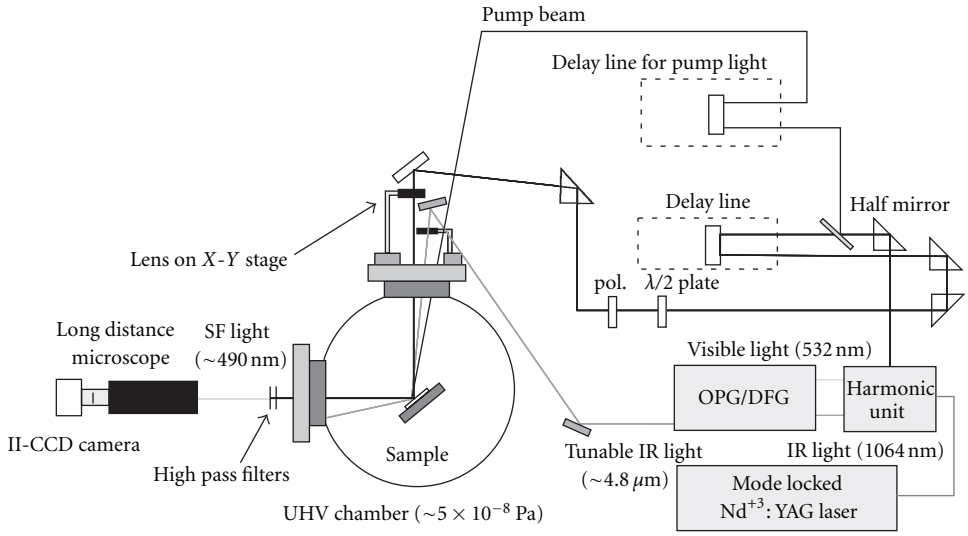

Figure 1: Schematic diagram of the SFG and SHG microscopic system for UHV conditions.

and dichroic filters to block the incident visible light and then introduced into a long-distance Cassegrain-type microscope (Quester QM-1). The microscope was equipped with a time-gated image-intensified charge-coupled device (CCD) camera (Hamamatsu PMA-100-H) for accumulating the SFG and SHG signals. With this long-distance microscope, the image of an object 0.5 m away can be focused on the detector plane with a resolution of $\sim 3\,\mu$m. The microscope was also equipped with bandpass filters with center wavelengths of 490 nm for SFG microscopy and 532 nm for SHG microscopy. The polarizations of the SFG, visible, and IR light were all, p, and p, respectively. For SFG spectroscopy, the SFG light was passed through a double monochromator, and detected by a photomultiplier and a gated integrator. The excitation light for SHG (with a wavelength of 1064 nm and power of $\sim 40\,\mu$J/pulse) was generated by the same OPG/OPA system as that used for the SFG measurements. The polarizations of the incident light and the SHG light were p and all, respectively. The integration time for taking both SFG and SHG intensity images was 500 seconds. It was confirmed that luminescence signals were very weak under these measurement conditions.

In developing this SFG and SHG microscopic system, we paid special attention to the following points. Our previous SHG microscope had a problem in that the images were modified by the nonuniform intensity distribution in the beam pattern of the incident light [23]. In order to avoid this modification, we moved the irradiating position on the sample in the luster scan by moving the focusing lenses, using an automatic X-Y stage. It is difficult to take the SFG and SHG microscopic images in exactly the same conditions, since incident light beams from different sources must be focused on the same area on the sample surface. In order to make the spot positions of the incident light beams exactly the same, we switched the optical paths of the incident light for SH microscopy and that of the incident visible light for SFG microscopy using a prism beam exchange mechanism. With these innovations, we succeeded in taking simultaneous SFG and SHG intensity images. The resolution of the microscope is $\sim 5\,\mu$m.

Section 4 shows SFG and SHG images of hydrogen deficiency on a Si(111) surface. In order to promote hydrogen desorption, the Si surface was irradiated with IR light pulses (wavelength: 1064 nm, pulse duration: $\sim 6\,\mu$s, repetition rate: 10 Hz, pulse energy: 6~12 mJ/pulse, focus size: ~0.1 mm) from a Nd^{3+}: YAG laser.

Section 5 presents the results of pump-probe SFG microscopy. The power of the pump visible light with wavelength 532 nm was $120\,\mu$J/pulse and the power density on the sample surface was $0.12\ \text{J/cm}^2\cdot$pulse. The pump light was nearly p-polarized and had the incident angle of 68.5°. The optical delay of the probe visible and infrared pulses was controlled by an automatic linear stage with the positioning accuracy of $\sim 5\,\mu$m. The timing of the pump and probe light was adjusted by monitoring the SFG of the pump visible and probe IR light from the sample with its surface tilted differently from the final SFG measurement. In the final SFG measurement, this SF light did not hit the detector because it traveled off the optical path at an angle of ~30°. No damage was observed in the linear microphotograph of the sample surface after the pump light irradiation. The invariance of the Si–H vibrational peak in the SFG spectra before and after the pump-probe measurement indicated the absence of the change of hydrogen coverage and disorder of the Si–H bonds during the strong pump light irradiation.

To prepare a H–Si(111)1 × 1 surface, n-type Si(111) wafers were etched in a clean room by a few cycles of dipping in a hot solution of 97% H_2SO_4 : 30% H_2O_2 = 4 : 1, then in hydrofluoric acid, and finally in NH_4F solutions to produce monohydride terminated Si(111) surfaces [4]. After this treatment, the sample was immediately introduced into the UHV chamber with a base pressure 5×10^{-8} Pa. A low-energy electron diffraction (LEED) measurement confirmed the 1 × 1 structure of the H–Si(111) surface thus prepared.

In the measurement of temperature dependency described in Section 6, DC current in the UHV chamber directly heated the sample. After heating for 10 s, the sample was cooled down to RT and SFG spectra and images were taken.

4. Images of Hydrogen Deficiency on a H–Si(111) Surface after Laser Pulse Irradiation

Laser CVD is a useful method for depositing high-quality thin film on a Si surface with low temperature [12]. One of the crucial processes in CVD is hydrogen desorption. The hydrogen desorption promoted by the rapid temperature rise on a Si surface after light pulse irradiation is known as laser-induced thermal desorption (LITD). In the laser CVD, growth of a uniform film, spatial uniformity of coverage and the orientation of H–Si bonds are important. However, because LITD is an indirect process, the spatial distribution changes dramatically as a function of the power density, wavelength, and duration of the incident light pulse [23, 34]. One must also consider the effect of electron-hole plasma excitation on the hydrogen desorption [23]. From these aspects, we used SFG and SHG microscopy to observe the spatial distribution of hydrogen deficiency on a H–Si(111) surface after laser pulse irradiation.

4.1. Source for LITD Process. Usually an Excimer laser with wavelength 193∼351 nm and pulse duration ∼25 ns is used as the source for a laser CVD process. However, we suggest that light pulses with longer pulse duration and longer penetration depth are more suitable. In the LITD process, the rapid temperature increase due to laser pulse irradiation causes not only hydrogen desorption but also, in some cases, surface melting. The surface melting changes the surface structure and may affect the quality of a deposited film.

In order to select the most suitable source for the LITD method, we calculated temperature change and hydrogen desorption after laser pulse irradiation. Through this simulation, we found that an IR light pulse with wavelength 1064 nm and pulse duration ∼6 μs can induce hydrogen desorption from a Si(111) surface without melting.

The calculation using the LITD model was based on a paper by Koehler and George [34], and an original source code programmed in our previous study [24]. In order to estimate the temperature of the Si surface, three-dimensional thermal diffusion was simulated by the finite difference method. The equation of thermal diffusion is

$$\frac{\partial T}{\partial t} = D\nabla^2 T + \mathrm{Q}, \tag{3}$$

where T is the temperature [K], t is the time [s], D is the thermal diffusivity [cm^2/s], and Q is the source term [K/s]. For calculating the source term, we adopted an absorption coefficient of 7.876 [35] and reflectivity of $0.311 + 5.0 \times 10^{-5} \times (T - 300)$ [35, 36]. The initial surface temperature was assumed as 300 K, since the advantage of laser CVD is availability of deposition at such a low temperature. The melting of Si bulk occurs at ∼1684 K [34, 35]. We note that the surface temperature is ∼1414 K [36, 37] and that a real Si surface melts with lower temperatures than the supposed temperature of this simulation. However, the difference in temperatures is not critical for comparing calculated and experimentally measured hydrogen coverage. Thus, in the simulation, the upper limit of the temperature was 1684 K, and the absorption coefficient, the reflectivity, the heat capacity, the thermal conductivity, and the density changes occur at this temperature [34].

The coverage change on the Si surface in the desorption kinetics is given by [34]

$$\frac{d\theta}{dt} = -\theta^n \nu_d \exp\left(-\frac{E_d}{RT_{\mathrm{surf}}}\right), \tag{4}$$

where θ is the coverage, E_d is the activation energy, R is the gas constant (8.31 J/molK), and T_{surf} is the temperature of the surface. The superscript n is the order of the desorption. The desorption order of a monohydride from a Si(111)7 × 7 surface greater than than 0.04 ML is assigned as second order [3, 38]. Hence, the order is treated as second order in this section. (In Section 6, we assume 0th-to-2nd-order desorption.) The surface temperature as a function of time was obtained by (3), and it was input into T_{surf} in (4). Solving (4) numerically, we obtained the time dependence of the hydrogen coverage θ.

The maximum surface density of the hydrogen atoms on a Si(111) surface corresponding to ∼1 ML equals 8×10^{14} cm^{-2} [34]. The activation energy E_d and the pre-exponential factor ν_d were set as 2.65 eV and 12 cm^2/s, respectively [34].

Figure 2(a) shows the simulated change in temperature and hydrogen coverage after a laser pulse irradiation with wavelength 355 nm, power 50 μJ/pulse, spot size 294 μm, and pulse duration 35.3 ps. Soon after the UV light pulse irradiates the Si surface at 0 s, the temperature shown as a gray curve in the figure increases to melting temperature (1684 K) and is then gradually reduced. On the other hand, the hydrogen coverage (black curve) is reduced only when the surface reaches melting temperature. This result indicates that hydrogen desorption is associated with surface melting after UV light pulses irradiation.

Figure 2(b) depicts the change of temperature and hydrogen coverage induced by an IR light pulse with wavelength 1064 nm, pulse duration 5.88 μs, power 10 mJ/pulse, and spot size 35.3 μm. The temperature (gray curve) increases to 1300 K after the IR light pulse irradiation at 0 s and is then gradually reduced. In Figure 2(b), the hydrogen coverage (black curve) is clearly reduced. This result shows that IR light can induce hydrogen desorption without melting.

Hydrogen molecular desorption occurs when the surface temperature is over ∼800 K [3]. Thus, in order to induce hydrogen desorption, temperatures higher than 800 K must be maintained for a long time. The key factors in heating time are penetration depth and pulse duration. UV and IR light penetrate Si at depths of ∼10 nm and 1 cm, respectively. UV light irradiation produces a rise in temperature only at the thin layer near the surface; the heat at that layer then diffuses to the rest of the sample. On the other hand, IR light, with its longer penetration depth, heats up the whole sample, and

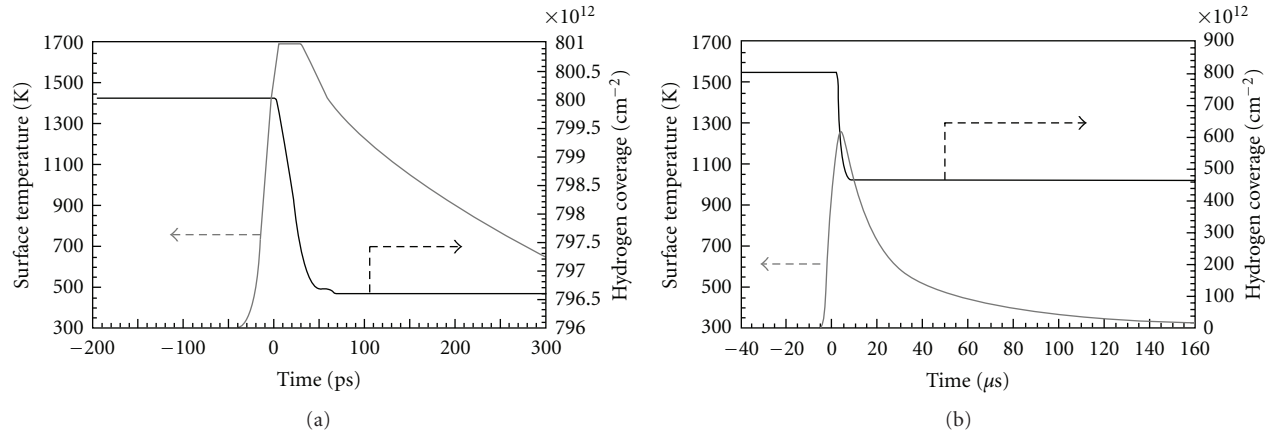

Figure 2: Temperature change and the reduction of hydrogen coverage after laser pulse irradiation with (a) wavelength 355 nm and pulse duration 30 ps, and (b) wavelength 1064 nm and ~6 μm.

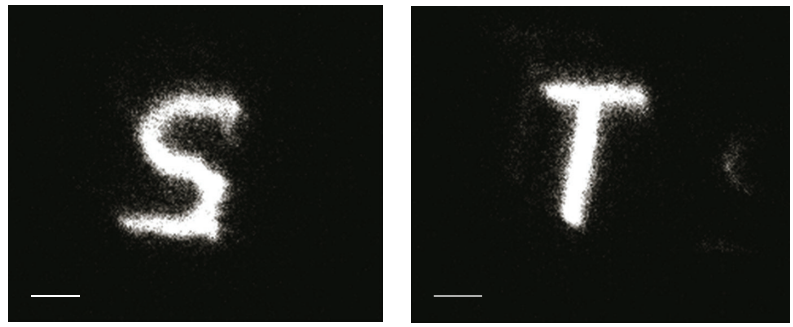

Figure 3: SHG intensity images of a H–Si(111) surface after IR light pulse irradiation with scanning character patterns "*S*" and "*T*," shown in (a) and (b), respectively. Scale bars are 200 μm.

thus the temperature at the surface reduces more gradually between pulses. Moreover, the pulse duration of IR light is 10^7 times longer than that of UV light, enabling the IR light to heat for a far longer time. Due to these properties, the time allowed for hydrogen desorption after IR light pulse irradiation is 10^5 times longer than that after UV light irradiation.

4.2. SHG Images of Hydrogen Deficiency on a Si(111) Surface after IR Light Pulse Irradiation. In order to demonstrate that IR light can remove part of the adsorbed hydrogen atoms without surface melting, we obtained SHG microscopy imagery of the H–Si(111) surface after the IR light irradiation. Figures 3(a) and 3(b) show SHG intensity images of a H–Si(111) surface after IR light pulse irradiation. The bright character patterns "*S*" and "*T*" can be seen in Figures 3(a) and 3(b) respectively. The results are interpreted as follows. The UV light gave rise to hydrogen desorption from the H-Si(111) surface and produced dangling bonds. Since surface electronic levels created by the dangling bonds are formed around the Fermi level, the resonant optical transition mediated by these surface electronic levels becomes possible at the incident photon energy $\hbar\omega = 1.17$ eV ($2\hbar\omega = 2.33$ eV), enhancing SHG [8, 39, 40]. According to a theoretical study done by Gavrilenko and Rebentrost, a peak at $2\hbar\omega = 1.5$ eV in the spectra of $\chi^{(2)}_{zzz}$ for a Si(111)1 × 1 surface is mainly determined by two-photon resonance due to the optical transitions involving the surface state [40]. This peak has a tail until 3 eV, and thus SHG can be enhanced at $2\hbar\omega = 2.33$ eV. The SHG method was also used to study the surface states of a Si(111)7 × 7 surface [16, 17]. On the other hand, a H-terminated surface has no surface state in the energy bandgap. Thus, SHG enhancement due to the resonant optical transition of the surface states does not occur for a H-terminated Si surface at $\hbar\omega = 1.17$ eV.

We note that the SHG signals are also sensitive to surface melting [23, 24]. In our previous research, enhanced SHG light can be seen in an area irradiated with UV light pulses on a Si(111) surface and that light originated not only from the created dangling bonds, but also from surface melting [24]. In order to discover the origin of SHG signals shown in Figure 3, we investigated if the strong SHG signals in an area irradiated with IR light pulses disappeared after hydrogen exposure. Figures 4(a) and 4(b) show SHG intensity images of a H–Si(111) surface before and after IR light pulse irradiation. In Figure 4(b), one can see enhanced SHG light generated at the area irradiated with IR light pulses. After taking the SHG intensity image shown in Figure 4(b), the Si surface

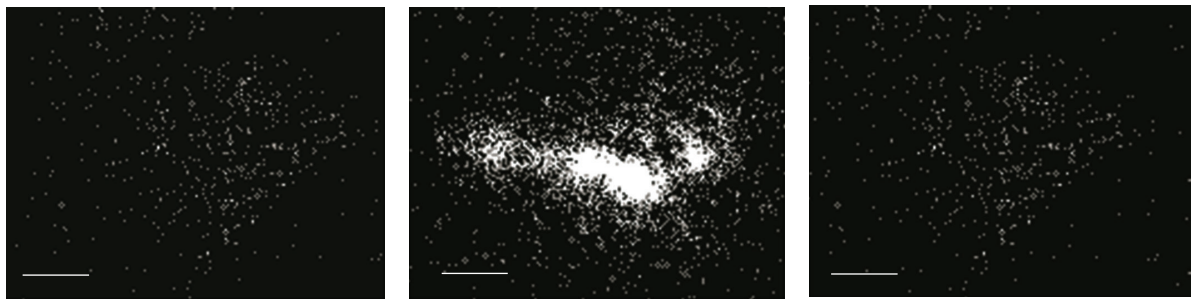

(a) (b) (c)

Figure 4: SHG intensity images of a H–Si(111) surface (a) before and (b) after IR light pulse irradiation, and (c) after hydrogen exposure to the Si surface. Scale bars are 200 μm.

was exposed to hydrogen molecules of ~3 torr for 5 minutes and then the molecules were evacuated again. It is noted that since the probability of hydrogen adsorption was very low at room temperature [9], the impure gas in the UHV chamber, for example, CO, CO_2, and H_2O molecules, might adsorb on the Si surface while it was being exposed to the hydrogen molecules. After the hydrogen exposure, an SHG intensity image was taken, as in Figure 4(c). In Figure 4(c), the SHG signals have disappeared completely. This result indicates that the Si surfaces were not melted by the IR light pulse irradiation.

4.3. SFG Microscopy of Hydrogen Species on a Si(111) Surface. In order to study the spatial distribution of Si–H bonds on a Si(111) surface after IR light pulse irradiation, we applied SFG microscopy to the surface. Hereafter, the IR light pulse for inducing hydrogen desorption will be referred to as "desorption inducer (di)-IR light pulse."

Figure 5 shows the SFG intensity spectrum of the H–Si(111)1 × 1 surface before and after di-IR light pulse irradiation. The black squares, gray triangles, and light gray circles, respectively, represent the SFG intensity of the H–Si(111) surface before, 10 minutes after, and 18 hours after the irradiation by the di-IR light pulses. The estimated exposure of the sample surface to impurity gas in 18 hours is ~27 L. The sharp peak at 2084 cm^{-1} in the spectrum of the Si surface before irradiation is attributed to the stretching vibration of the monohydride species. We note that Higashi et al. performed an ATR-IR measurement of a H–Si(111) surface (with a resolution of ~0.5 cm^{-1}) and determined that the peak at 2083.7 cm^{-1} was due to the Si–H stretching vibration of monohydride [4]. The probe light in our work has a bandwidth of ~6 cm^{-1}, so we cannot measure peaks with resolution better than ~6 cm^{-1}. Thus, the resonant peak observed at 2080~2085 cm^{-1} in our works was unified as 2084 cm^{-1} in this paper, following the vibration frequency observed by Higashi et al.

In the SFG spectrum of the surface 10 minutes after the irradiation, the peak at 2084 cm^{-1} disappeared and the SFG signal intensity was almost constant from 2060 to 2140 cm^{-1}. This result indicates that the SFG signals in the irradiated area did not occur due to resonance with any vibrational mode. In the SFG spectrum of the surface 18 hours after

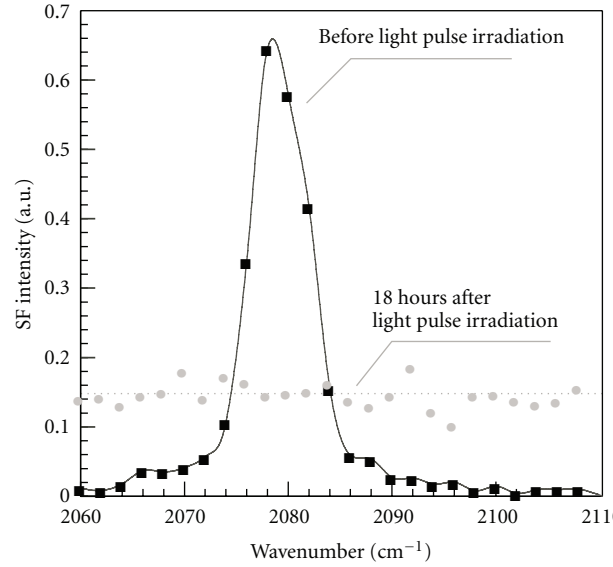

Figure 5: SFG intensity spectra of a H–Si(111)1 × 1 surface before (black squares), 10 minutes after (dark gray triangles), and 18 hours after (light gray circles) IR light pulse irradiation.

irradiation, the signal is uniformly weaker and has no peak (light gray circles in Figure 5). However, the SFG spectrum in the nonirradiated area did not change significantly even after 18 hours. Thus, the decrease of the nonresonant SFG signals in the irradiated area is due to the adsorption of the impurity gas in the UHV chamber. In another experiment, 90% of the SFG signals from the irradiated area disappeared after exposure to 1 atm of air. These results suggest that most of the SFG signals in the irradiated area are due to the surface electronic level associated with the dangling bonds formed after hydrogen desorption. We suggest that the signals may have been enhanced by an electronic transition caused by the IR probe light [28].

Figure 6(a) illustrates the three areas on the Si(111) surface irradiated by di-IR light pulses with several energies from 11 to 13 mJ/pulse. The ring represents the beam spot, and one light pulse was injected into each area. Figures 6(b) and 6(c) show the SFG intensity images of a H–Si(111)

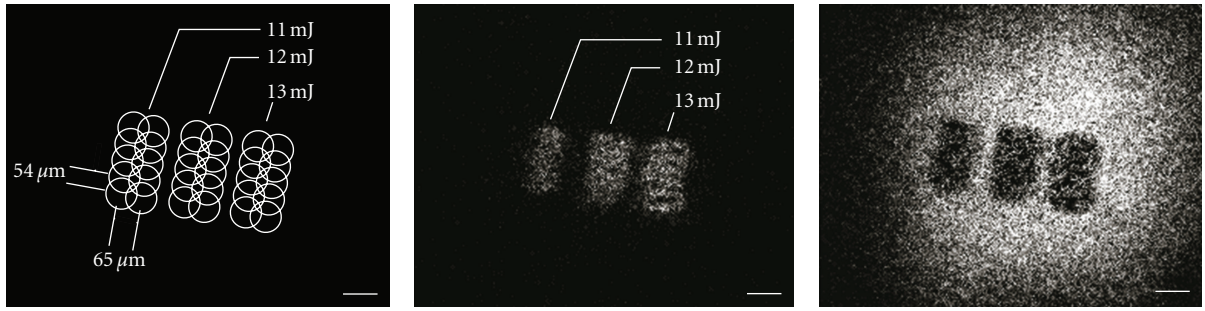

(a) (b) (c)

Figure 6: (a) A schematic illustration of three areas on a Si(111) surface irradiated by di-IR light pulses with energy from 11 to 13 mJ/pulse. Each ring pattern represents one laser beam spot, and a total of 10 light pulses were injected into each area. (b) and (c) show SFG intensity images of a H–Si(111) surface after irradiation by di-IR light pulses with IR probe light wavenumbers of 1954 cm^{-1} and 2084 cm^{-1}, respectively. The bright dots represent the observed SFG photons. Scale bars are 100 μm.

surface with IR probe light wavenumbers of 1954 cm^{-1} and 2084 cm^{-1}, respectively. In the SFG spectrum of the surface before the irradiation in Figure 4, the sharp peak at 2084 cm^{-1} is attributed to the stretching vibration of the monohydride. On the other hand, there was no vibrational resonance at 1954 cm^{-1}. Thus, Figures 6(b) and 6(c) represent nonresonant and resonant SFG intensity images with Si–H vibration, respectively. Hereafter, I will refer to nonresonant and resonant vibrational SFG signals as NR- and RV-SFG signals.

In Figure 6(b), one can see strong NR-SFG signals generated at the irradiated areas; these may originate from the dangling bonds created after the hydrogen desorption caused by the pulse light irradiation. Figure 6(c) shows an RV-SFG intensity image for the IR probe wavenumber 2084 cm^{-1}. In the original SFG intensity image with IR wavenumber 2084 cm^{-1}, the NR-SFG signal also appeared at the irradiated area, so we have subtracted these NR-SFG signals in Figure 6(b) from the total signal. In Figure 6(c), the RV-SF signals have disappeared in the irradiated areas. We note that there was damage in the area irradiated with the pulses of 13 mJ/pulse. The stripe patterns in the area irradiated by the pulses of 13 mJ/pulse in Figure 6(b) reflect the damage patterns.

We also note that the area emitting SFG light shown in Figure 6(b) is smaller than the spot size of the di-IR light pulses shown in Figure 6(a). In the LITD process, only a small area around the center of the pulse spot was heated to a high temperature ($\sim$1000 K), and thus the hydrogen molecules desorbed only in that area. This is why the area emitting an NR-SFG signal caused by a hydrogen deficiency in Figure 6(b) is smaller than the spot size seen in Figure 6(a).

In order to estimate the widths of the areas of the RV-SFG and NR-SFG signals, we fit Gaussian curves to the profiles of the observed SFG intensity images. The full width at half maximum (FWHM) of the areas of the profile of the NR-SFG signals irradiated with di-IR light pulses at 11, 12, and 13 mJ/pulse is estimated to be 53, 66, and 70 μm, respectively. On the other hand, the FWHMs of the dark areas in the RV-SFG signals are estimated to be 79, 87, and 81 μm, respectively. At each power of the di-IR light pulses, the width of the dark area in the RV-SFG signals is wider than that of the area emitting the NR-SFG signals. This result indicates that there is a boundary area between the RV and NR-SFG signal areas. Both the resonant and nonresonant signals were very weak in this boundary area. We suggest that at the boundary area, the orientation of the Si–H bonds was disordered and/or the desorption of hydrogen did not leave enough dangling bonds, so that neither the RV-SFG nor NR-SFG signals were strong [28].

5. Time-Resolved SFG Microscopy

We observed a change in the spatial distribution of hydrogen molecules after the LITD process described in the previous section. Under some light conditions, we found an unidentified bonding state of Si–H on the edges of the irradiated area in the SFG image. The dynamics of the electrons and phonons on the edges of the light pulse spot are complicated because the IR light pulse not only raises the surface temperature but also simultaneously excites the electron-hole (e-h) plasma. The e-h pair is excited by the IR light pulse with photon energy of 1.17 eV via indirect electron transition beyond the bandgap of silicon $\sim$1.1 eV [41]. If a high density of e-h pairs is excited, the medium is in a plasma state called e-h plasma. In order to clarify the dynamics at a particular part of this region, picoseconds-order snapshots of the hydride on a Si surface have to be taken after the pump light irradiation. Thus, the SFG microscope must be equipped with a pump-probe time-tracking function.

In this section, we demonstrate time-resolved- (tr-) SFG microscopy of a H–Si(111) surface under ultra-high vacuum conditions. We chose pump light with photon energy 2.33 eV and pulse width $\sim$30 ps, since this pump pulse not only gives rise to high surface temperature without desorption but also efficiently excites e-h plasma [41].

We note that Guyot-Sionnest studied a modification of the Si–H stretching vibration due to visible light with photon energy 2.33 eV irradiation by measuring time-resolved sum frequency spectra [41]. However, we are interested in modulating the Si–H stretching vibration by pump light irradiation with a fluence larger than $\sim$100 mJ/cm^2 as a basic study for Laser CVD, while Guyot-Sionnest used a power

of ∼50 mJ/cm^2. The modulation caused by the stronger power is expected to be different from that excited by the weaker, since a laser fluence higher than ∼100 mJ/cm^2 may cause not only Auger recombination but also plasmon-phonon-assisted recombination (PPAR) of the excited carriers [42]. Thus, our tr-SFG spectra are in themselves worthy of attention.

Figure 7 shows the SFG spectra at several delay times. The delay time is indicated on the right-hand side of each SFG spectrum. Before the pump light irradiation (−53 ps), a symmetric peak is seen at 2084 cm^{-1} attributed to the Si–H stretching vibration. After the pump light irradiation, three significant modifications are observed in the SFG spectra. First, the nonresonant signals jump up at 0 ps, and then decrease gradually. Second, from 0 to 66 ps, the peak rapidly decreases along with an increase of the nonresonant SFG signal background; from 66 to 930 ps, the peak gradually recovers. Third, at 930 ps, the peak has a remarkably asymmetric lineshape. None of these features except the rapid decrease of the resonant peak from 0 to 66 ps were observed by Guyot-Sionnest [41]. We discuss the origins of these three modifications below.

In order to analyze the change in the nonresonant SFG signal, we measured SFG intensity as a function of probe delay time with an IR wavenumber 2019 cm^{-1} as shown in Figure 8(a). The solid curve represents best exponential fitting curves. This IR probe wavenumber is in off-resonance to the surface Si–H vibrational frequency. In Figure 8(a), the signal jumps up at 0 ps and then decreases gradually with a life time of 565 ps.

The density of the e-h pairs excited by the pump pulses is estimated as $\sim 3 \times 10^{21}$ cm$^{-3}\cdot$pulse^{-1} and is high enough to create a plasma state. Thus, as one possible origin of the enhancement of the nonresonant SF signal at 0 ps, the e-h plasma may modify the dielectric constant of the Si substrate at the probe IR light frequency [41]. It has been reported that modulating the Fresnel factor for IR light enhances the SFG signal [41]. However, the lifetime of the plasma should be less than the ∼100 ps created by the Auger recombination or faster processes like PPAR [42]. This life time is not compatible with the observed life time of the signal. On the other hand, the modulation of Fresnel factors for visible and SFG light by the plasma is negligible [9, 41].

A second candidate origin may be the effect of the temperature rise on the Si surface. Guyot-Sionnest pointed out that surface temperature rises immediately after the visible excitation and is kept constant within the timescale of 500 ps. The high-density phonons excited in the quasithermal equilibrium may induce some broad second-order nonlinearity. However, the nonresonant signal was not reported with the laser power used by Guyot-Sionnest [41]. Thus, the nonresonant signal observed in this work must be attributed to the high fluence of the visible pump light.

As a third candidate, the nonlinear susceptibility $\chi^{(2)}_{\mathrm{NR}}$ in (1) may have been enhanced by the electric field accompanying the e-h pairs excited at 0 ps, due to the electric-field-induced sum frequency generation [43]. After that, the susceptibility $\chi^{(2)}_{\mathrm{NR}}$ may have decreased due to the relaxation of the e-h pairs. As we mentioned above, the number of the excited carriers is reduced via Auger recombination or a PPAR process in ∼100 ps, but a small amount of carriers should remain after the recombination. According to our calculations, the remaining carriers diffuse slowly after ∼100 ps. The order of the life time is consistent with the observed life time of the signal in Figure 8(a). We also note that no background SFG signal was observed for the ssp polarization combination (s-polarized SFG, s-polarized visible, and p-polarized IR) in a separate experiment. This result suggests that the nonresonant background signal observed for the ppp polarization combination in Figure 8(a) does not originate from any trivial optical process such as scattering due to surface damages.

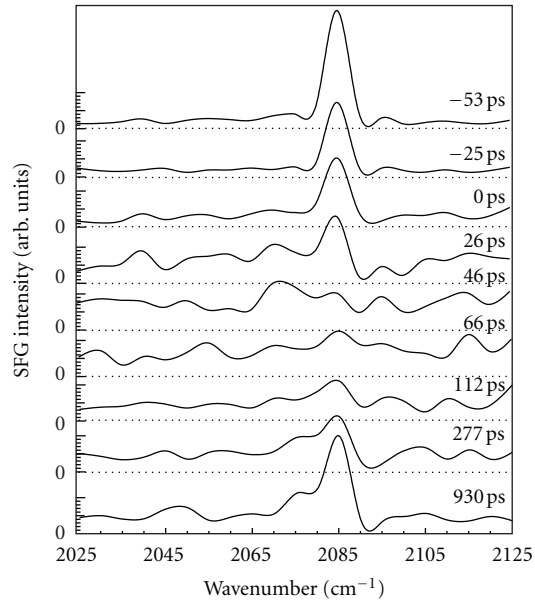

Figure 7: SFG intensity spectra of a H–Si(111) surface at several probe delay times with respect to pump visible pulses of photon energy 2.33 eV. The delay times are indicated on the right hand side of each SFG intensity spectrum.

Figure 8(b) shows the SFG signal as a function of delay time with the IR wavenumber 2084 cm^{-1}. The SFG signal contains both the resonant and nonresonant contributions. Contrary to the change of the nonresonant SFG signal, this signal drops down to half of its initial value at 0 ps and slowly recovers with a lifetime of 305 ps. This result indicates that the Si–H stretching vibration is modulated strongly after pump light irradiation.

In our calculation, the surface temperature reaches ∼500 k at 20 ps after the pump light irradiation. With the temperature increase, the damping constant Γ of the resonant term in (2) may increase because of weak anharmonic coupling between the Si–H vibration and the optical phonon of ∼200 cm^{-1} [41]. Thus, the peak of the Si–H stretching vibration is considered to drop due to the broadening. In addition, since the surface temperature is over 300 K, the strong anharmonic coupling with the bending mode may also modify the Si–H stretching vibration [44]. In this study, the peak of the Si–H vibration disappears at 46 ps in Figure 7, while

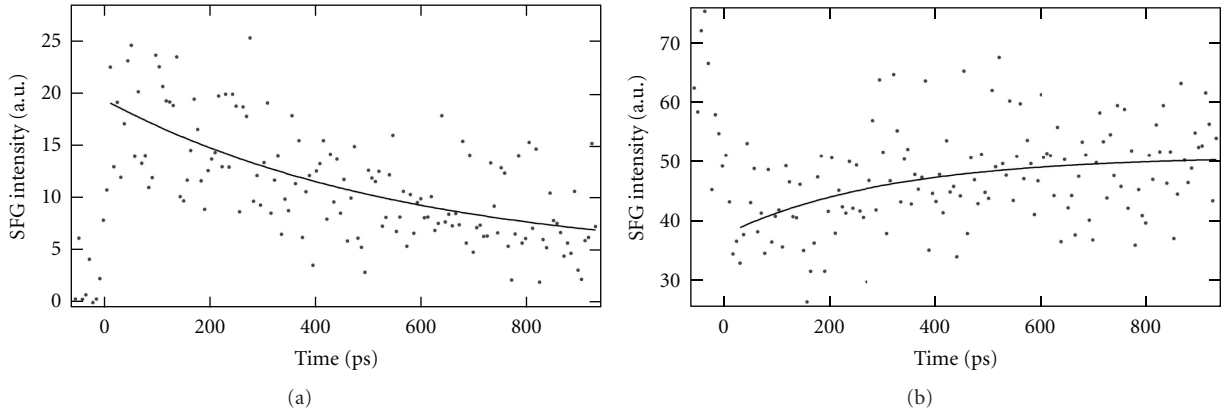

Figure 8: SFG intensity as a function of the probe delay time of the visible and IR pulses with respect to the pump visible pulses. The IR light wavenumbers are (a) 2019 cm^{-1} and (b) 2084 cm^{-1}. Solid curves represent a guide to the eye.

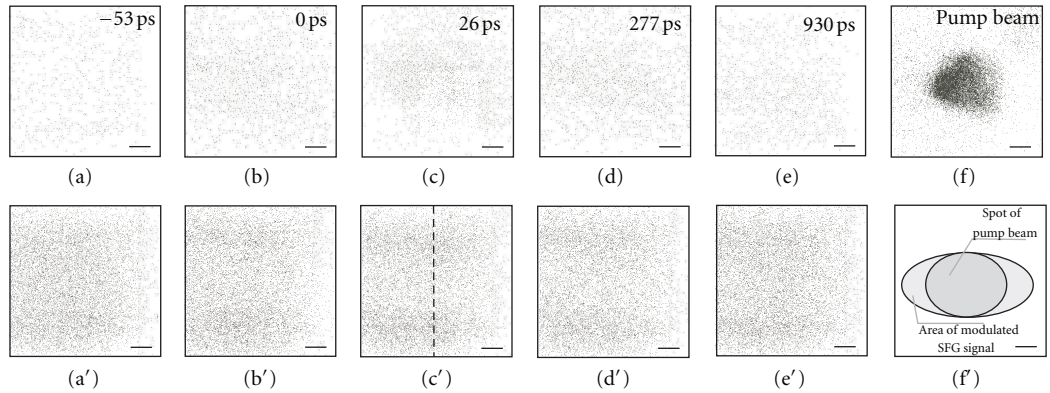

Figure 9: (a)∼(e) Nonresonant and (a′)∼(e′) resonant SFG images as a function of delay times from 0 to 930 ps with IR light wavenumbers 2019 and 2084 cm^{-1}. (f) The resonant SFG intensity images corresponding to the pump light spot. (f′) A schematic illustration of expanded areas of modulated SFG signals compared to pump spot size. Scale bars are 200 μm.

in the work of Guyot-Sionnest [41], the signal was more than a half of the initial intensity at every delay time after the light pulse irradiation. Indeed, the stronger excitation gives rise to more severe modification of the Si–H vibration. Unfortunately, however, we cannot estimate the change of the damping constant Γ and the peak shift after the pump light irradiation due to the insufficient signal to noise ratio in our results.

The asymmetric lineshape at 930 ps in Figure 7 could originate from a nonuniform temperature drop on the surface. However, as pointed out by Guyot-Sionnest [41] and in our previous theoretical work [24], the temperature drop should be very slow after the jump to 500 K at 20 ps. For instance, the temperature is still calculated to be 483 K at 500 ps. The Si surface is in quasithermal equilibrium up to 1 ns, so temperature change is not expected to result in a peak recovery and change in the lineshape. In order to understand the recovery of the peak and the origin of the asymmetric lineshape, further theoretical study is necessary.

In obtaining tr-SFG microscopy imagery, we estimated the pump spot size by observing an SFG intensity image of the Si surface with the incident IR light and pump visible light. Figure 9(f) shows the SF intensity image reflecting spatial distribution of the pump spot. With Gaussian fitting of the profile, we estimated the FWHM of the pump spot as $304 \pm 2\,\mu$m.

At several delay times from −53 to 930 ps after the pump light irradiation, we observed nonresonant and resonant SFG intensity images of the Si surface. Figures 9(a) to 9(e) show nonresonant SFG intensity images of the area irradiated by the pump light on the Si surface with IR light of 2019 cm^{-1} and delay times from −53 to 930 ps. The dark dots in Figure 9 represent SFG photons. In Figures 9(a) to 9(e), the number of nonresonant SFG photons at the pump-irradiated area increased from 0 to 26 ps, and then decreased gradually. On the other hand, Figures 9(a′) to 9(e′) show the change in the resonant SFG intensity images with IR light of 2084 cm^{-1}, and delay times of −53 to 930 ps. In Figures 9(a′) to 9(c′), the number of resonant SFG photons decreases due to the pump light irradiation and then recovers from Figure 9(c′) to 9(e′).

The changes in the SFG signals are consistent with the results of one-point tr-SFG measurement. However, the anistropic expansion in the areas of modulated SFG signals

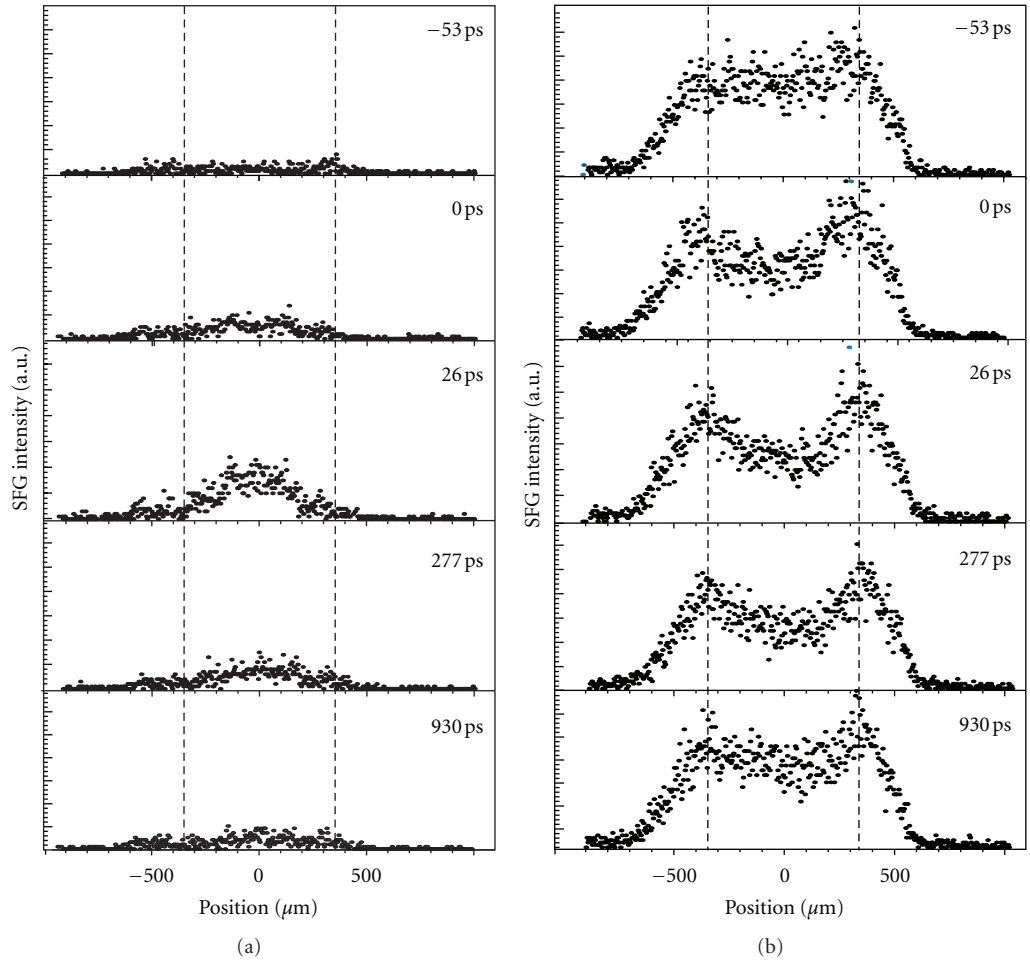

Figure 10: The profiles of the time-resolved SF intensity images with pump photon energy 2.33 eV; (a) the nonresonant signal with IR wavenumber 2019 cm^{-1}; (b) the resonant signal with IR wavenumber 2084 cm^{-1}.

at 277 ps, shown in Figure 9(d) and 9(d′), is surprising. As seen in Figure 9(f′), the area of modified SFG is ∼ two times as large as the pump spot size. This is not due to carrier diffusion, since the diffusion constant is ∼20 cm^2/s [45], and thus the carriers diffuse in only 2 μm at 1 ns after pump light irradiation. Moreover, in our calculation, in-plane propagation of heat is also negligible. The phenomenon may be related to phonon-phonon and/or phonon-vibration coupling at the surface with temperature gradient; the analysis of these images is under way.

Figure 10 shows profiles of the SFG intensity obtained from the nonresonant and resonant SFG intensity images in Figure 9 with the positions shown as a dashed line in Figure 9(c′). The vertical and horizontal axes in Figure 10 represent the SFG intensity and the position on the sample, respectively. A significant change in the SFG signals was observed in the area between vertical dashed lines, at positions of ±350 μm. The FWHM of the non-resonant SF signal at −53 ps is 1363 μm; it then narrows to 436 μm at 26 ps. After 26 ps, the FWHM increases gradually, becoming 673 μm at 930 ps. The FWHM broadens as a function of delay time after 0 ps. Carrier diffusion along the surface could not be a possible origin of the broadening due to the low diffusivity [45]. As another possibility, the broadening may represent a different decay time for each position, corresponding to the spatial distribution of pump light intensity. At the center area irradiated by pump pulses with high fluence, a number of e-h pairs were generated, and thus the pairs quickly decayed due to Auger recombination or PPAR processes. On the other hand, a handful of e-h pairs were generated by pump pulse irradiation with low fluence at the outer area. The decay time of the outer area should be slower than that in the center, and thus FWHM could broaden as a function of time due to the difference in decay times.

6. Hydrogen Diffusion on a Si(111)1 × 1 Surface

Hydrogen diffusion on a Si surface is a topic of great interest. For example, in an isothermal desorption from a Si(111)7 × 7 surface studied by Reider et al. [38], the desorption order changed from 2 to 1.5 when the coverage was lower than 0.04 ML. They suggested that an appropriate modified model that includes the possibility of island formation is required for understanding the intermediate kinetic order. Thus,

the diffusivity of hydrogen has been measured by LITD [3] and optical SHG light diffraction [18]. However, neither anisotropy nor the island structure of hydrogen distribution was observed directly in those works, even though these factors are key to understanding the intermediate kinetic order. For studying anisotropic diffusion, a microscopic approach is necessary.

In this section, we demonstrate the usefulness of SFG microscopy for observing hydrogen diffusion. We note that the scale of the diffusivity of hydrogen atoms on a Si surface is smaller than the resolution of present SFG microscopes ($\sim 5\,\mu$m), and thus the diffusion was difficult to observe directly with our microscope. However, if there are roughness areas of micron size, the SFG microscopy can show the influence of those areas on the hydrogen diffusion and desorption processes. According to a study by RHEPD, there are roughness areas including trihydrides on a Si(111)1 × 1 surface, even though the size of the areas is unknown [11]. When temperature is increased to desorption temperature, ~740 K, the hydrogen diffusion and desorption processes of the areas are different from those in areas adsorbed by well-ordered mohydride species. Thus, the spatial distribution of hydrogen atoms would be inhomogeneous with progression of the desorption dynamics due to the different processes in these areas. In order to study the change in spatial distribution on the surface with increased temperature, we used SFG microscopy for our observations.

In order to confirm the hydrogen desorption order of the 1 × 1 surface, we first studied the time dependence of isothermal desorption at temperatures 711, 732, 752, and 771 K by taking SFG spectra. It should be noted that the desorption order of the 1 × 1 surface has not been well studied. DC current in the UHV chamber directly heated the sample. After heating for 10 s, the sample was cooled down to RT and an SFG spectrum was taken.

We assume that the hydrogen coverage N can be estimated approximately from the peak height of SFG peaks with homogeneous width and Lorentzian shape as

$$N \propto A_q = \sqrt{I_p}\ \times \Gamma, \tag{5}$$

where I_p is peak height, and A_q and Γ are the strength and damping terms in (2), respectively. Generally, the area intensity of a peak in an SFG spectrum is not proportional to the coverage [46]. However, the SFG peaks at 2084 cm^{-1} were symmetric in all the observed spectra, and the contribution of the nonresonant term to SFG spectra was judged to be negligible. Only under such a condition can the coverage be approximately estimated as $A_q = \sqrt{I_p}\ \times \Gamma$, since the integral of the imaginary part of susceptibility per molecule should be constant when Γ is a homogeneous width. In this way, the hydrogen coverage was approximately evaluated for the SFG spectra. We note here that all SFG spectra were fitted by Gaussian functions since peaks at low coverages after long-time heating could not be fitted by Lorentzian functions. This indicates that the intensity data are unreliable at low coverage (~0.2 ML).

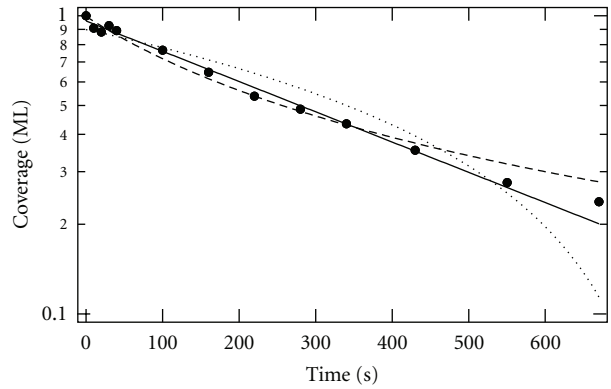

Figure 11: Isothermal hydrogen desorption from the H–Si(111) surface with a surface temperature of 711 K The points are experimental results. The dotted curve, solid line, and dashed curve are the zeroth, first, and second order of hydrogen desorption.

Figure 11 represents the time dependence of hydrogen coverage at a heating temperature of 711 K. The solid dots correspond to the coverage at each experimental point taken after the net heating time shown on the horizontal axis. The dotted, dashed, and solid curves represent the hydrogen desorption fitted with zero, first, and second orders, respectively. The hydrogen coverage decreased from 1 to ~0.2 ML in ~700 s. The isothermal desorption spectra at 732, 752, and 771 K also showed similar decay. Around ~0.2 ML, the resonant SFG signal became comparable to the nonresonant background, and the intensity data are unreliable. Moreover, generally above 0.04 ML, one cannot distinguish which order will be the best fit [38]. Thus, we could not determine the desorption order due to the unreliability at ~0.2 ML. Within the precision of our measurements, the results are compatible with the reported second-order kinetics on a 7 × 7 surface [3, 47, 48].

In order to observe the inhomogeneous distribution of hydrogen atoms caused by the existence of roughness areas, we observed SFG intensity images of the H–Si(111) surface as a function of heating temperatures from 592 to 752 K, as shown in Figure 12. The white dots represent SFG photons. We observed a gradual decrease in SFG intensity from 592 K to 752 K. An especially dramatic reduction of the SFG photon density was observed between 666 K (Figure 12(c)) and 728 K (Figure 12(d)); finally, the observed number of photons at 752 K in Figure 12(e) was close to the nonresonant background shown in Figure 12(f). We interpret the reduction of the SFG signal as simply the result of a deficiency in hydrogen atoms, taking account of the fact that the surface still has a 1 × 1 structure at temperatures lower than 770 K [49], and thus the molecular orientation has not changed.

Here, it is important to note that the number of SFG photons has been reduced homogeneously at 728 K in Figure 12(d). Fourier transform analysis of this image also supports that there are no significant structures. These results suggest that there was no island structure [11] and the hydrogen atoms diffused homogeneously with our microscope's estimated spatial resolution of $\sim 5\,\mu$m. If the size of the roughness areas observed by RHEPD is micron scale, the SFG

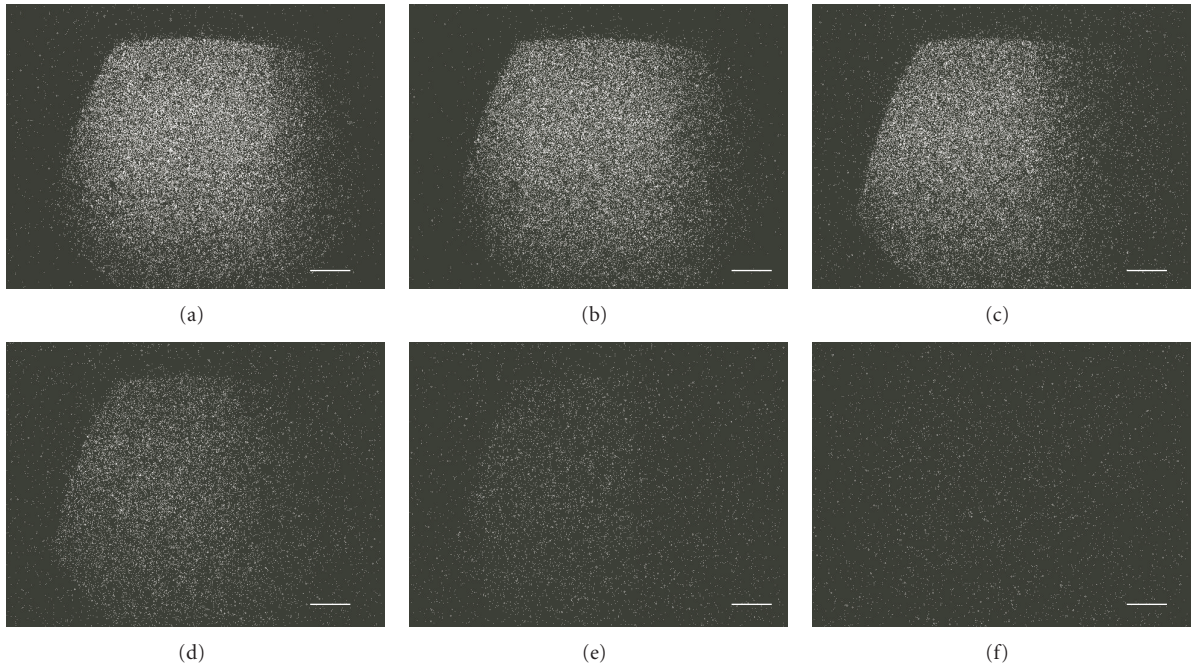

Figure 12: Resonant SFG intensity images at 2084 cm^{-1} of the H/Si(111) surface after heating for 10 s to several temperatures: (a) 592 K, (b) 625 K, (c) 666 K, (d) 728 K, and (e) 752 K. (f) A nonresonant SFG image at 2060 cm^{-1} of the surface after heating to 744 K. Scale bars are 100 μm.

images should be inhomogeneous. These results, therefore, indicate that the size of the roughness areas is at least smaller than 5 μm.

It has been reported that the diffusivity of hydrogen atoms on a Si(111)7 $\times$ 7 surface is 5 $\times$ 10^{-14} cm^2/s at 740 K [18, 50], which means that a hydrogen atom moves ~20 nm per 10 seconds during heating at 740 K. Moreover, the diffusion barrier of an unreconstructed 1 $\times$ 1 surface may be higher than that of a 7 $\times$ 7 surface, and thus the diffusivity of the 1 $\times$ 1 surface can be presumed to be slower. Thus, the scale of hydrogen diffusion is under the resolution limit of present microscopes. Future development of a microscope with better resolution will enable us to directly observe the change of hydrogen distribution due to the diffusion of hydrogen atoms.

7. Conclusions

This review has introduced some applications of second-order nonlinear microscopy to the observation of a H-Si(111)1 $\times$ 1 surface in UHV conditions. As the basic study for laser CVD, we took SFG and SHG microscopic images of the surface after IR light pulse irradiation. The light pulses with pulse duration ~6 μs can induce hydrogen desorption without surface melting, and may be used in laser CVD processes for the deposition of high-quality film. We have found that after irradiation by IR light pulses the SHG signals were enhanced due to the formation of dangling bonds after hydrogen desorption. Nonresonant SFG signals also appeared after the irradiation. By observing the spatial distribution of resonant and nonresonant SFG signals, we found an unidentified bonding state on the edges of the irradiated area in some light conditions. Both the resonant and nonresonant signals were very weak in this area.

In order to clarify the modulation of Si–H bonds induced by light pulses, we observed time-resolved SFG intensity images of a H–Si(111)1 $\times$ 1 surface. After visible pump light irradiation, nonresonant SFG signal increased at probe delay time 0 ps, and then decreased over a life time of 565 ps. The resonant SF signal with 2084 cm^{-1} reduced dramatically at 0 ps and then gradually recovered with an anisotropic line shape over a life time of 305 ps. The areas of modulated SFG signals at delay time 277 ps were expanded with an anisotropic aspect.

We also observed SFG intensity images of hydrogen deficiency on a Si(111)1 $\times$ 1 surface as a function of temperature. The SFG intensity images of the H–Si(111) surface, with a spatial resolution of 5 μm at several temperatures from 572 to 744 K, showed that the hydrogen desorbs homogeneously.

Based on our results, we suggest that the spatial distribution of hydrogen coverage or the orientation of the Si–H bonds dynamically affects the properties of an epitaxial thin film during laser CVD growth. Thus, the new bonding state found in this study increases our knowledge of the hydride change in CVD growth and could lead to the development of new devices, such as solar cells with improved light-induced degradation properties. The present study also demonstrates that SFG and SHG microscopes are useful tools, not only for observing the light pulse modification of a Si–H bonds, but also for studying hydrogen diffusion on a Si surface.

Acknowledgment

The author would like to thank Professor G. Mizutani and Ms. K. Hien of Japan Advanced Institute of Science and Technology, and Professor H. Sano of Ishikawa National College of Technology for their valuable advice and support. This work was supported in part by a Grant-in-Aid for Scientific Research (C) of Japan Society for the Promotion of Science (no. 23540363).

References

[1] J. A. Del Alamo, "Nanometre-scale electronics with III-V compound semiconductors," *Nature*, vol. 479, no. 7373, pp. 317–323, 2011.

[2] A. H. Mahan, Y. Xu, D. L. Williamson et al., "Structural properties of hot wire a-Si:H films deposited at rates in excess of 100 Å/s," *Journal of Applied Physics*, vol. 90, no. 10, pp. 5038–5047, 2001.

[3] B. G. Koehler, C. H. Mak, D. A. Arthur, P. A. Coon, and S. M. George, "Desorption kinetics of hydrogen and deuterium from Si(111)7 × 7 studied using laser-induced thermal desorption," *The Journal of Chemical Physics*, vol. 89, no. 3, pp. 1709–1718, 1988.

[4] G. S. Higashi, Y. J. Chabal, G. W. Trucks, and K. Raghavachari, "Ideal hydrogen termination of the Si (111) surface," *Applied Physics Letters*, vol. 56, no. 7, pp. 656–658, 1990.

[5] J. J. Boland, "Nature of the hydride species on the hydrogenated Si(111)-(7×7) surface," *Journal of Physical Chemistry*, vol. 95, no. 4, pp. 1521–1524, 1991.

[6] D. Lin and R. Chen, "Hydrogen-desorption kinetic measurement on the Si(100)-2 × 1:H surface by directly counting desorption sites," *Physical Review B*, vol. 60, no. 12, pp. R8461–R8464, 1999.

[7] V. De Renzi, R. Biagi, and U. Del Pennino, "Study of the transition from the ideal Si(111)-H(1×1) surface to the (7×7) reconstruction by HREELS, UPS and LEED," *Surface Science*, vol. 497, no. 1–3, pp. 247–253, 2002.

[8] P. Bratu and U. Höfer, "Phonon-assisted sticking of molecular hydrogen on Si(111)- (7 × 7)," *Physical Review Letters*, vol. 74, no. 9, pp. 1625–1628, 1995.

[9] M. Y. Mao, P. B. Miranda, D. S. Kim, and Y. R. Shen, "Characterization of hydrogen-terminated Si(111) surfaces by sum-frequency surface vibrational spectroscopy," *Applied Physics Letters*, vol. 75, no. 21, pp. 3357–3359, 1999.

[10] S. Ye, T. Saito, S. Nihonyanagi et al., "Stability of the Si-H bond on the hydrogen-terminated Si(1 1 1) surface studied by sum frequency generation," *Surface Science*, vol. 476, no. 1-2, pp. 121–128, 2001.

[11] A. Kawasuso, M. Yoshikawa, K. Kojima, S. Okada, and A. Ichimiya, "Rocking curves of reflection high-energy positron diffraction from hydrogen-terminated Si(111) surfaces," *Physical Review B*, vol. 61, no. 3, pp. 2102–2106, 2000.

[12] M. Tsuji, K. Kobarai, S. Yamaguchi, H. Obase, and Y. Nishimura, "Dissociative excitation of SiH4 by collisions with krypton active species," *Chemical Physics Letters*, vol. 166, no. 5-6, pp. 485–490, 1990.

[13] K. Ishikawa, K. Ueda, and M. Yoshimura, "New development of scanning-type microscope for two-dimensional hydrogen distribution using electron-stimulated desorption method," *Surface Science*, vol. 433, pp. 244–248, 1999.

[14] Y. R. Shen, *The Principles of Nonlinear Optics*, Wiley, New York, NY, USA, 1984.

[15] T. F. Heinz, M. M. T. Loy, and W. A. Thompson, "Study of Si(111) surfaces by optical second-harmonic generation: reconstruction and surface phase transformation," *Physical Review Letters*, vol. 54, no. 1, pp. 63–66, 1985.

[16] U. Höfer, "Nonlinear optical investigations of the dynamics of hydrogen interaction with silicon surfaces," *Applied Physics A*, vol. 63, no. 6, pp. 533–547, 1996.

[17] T. Suzuki, "Surface-state transitions of Si(111)-7 × 7 probed using nonlinear optical spectroscopy," *Physical Review B*, vol. 61, no. 8, pp. R5117–R5120, 2000.

[18] G. A. Reider, U. Höfer, and T. F. Heinz, "Surface diffusion of hydrogen on Si(111)7 × 7," *Physical Review Letters*, vol. 66, no. 15, pp. 1994–1997, 1991.

[19] J. Price, Y. Q. An, P. S. Lysaght, G. Bersuker, and M. C. Downer, "Resonant photoionization of defects in $Si/SiO_2/HfO_2$ film stacks observed by second-harmonic generation," *Applied Physics Letters*, vol. 95, no. 5, Article ID 052906, 2009.

[20] A. Wirth, J. Wei, J. J. H. Gielis et al., "Second-harmonic spectroscopy of Si nanocrystals embedded in silica," *Physica Status Solidi C*, vol. 5, no. 8, pp. 2662–2666, 2008.

[21] Y. Q. An, R. Carriles, and M. C. Downer, "Absolute phase and amplitude of second-order nonlinear optical susceptibility components at Si(001) interfaces," *Physical Review B*, vol. 75, no. 24, Article ID 241307, 2007.

[22] Y. Sonoda, G. Mizutani, H. Sano, S. Ushioda, T. Sekiya, and S. Kurita, "Ultra-high vacuum optical second harmonic microscope," *Japanese Journal of Applied Physics Part 2*, vol. 39, no. 3, pp. L253–L255, 2000.

[23] Y. Miyauchi, H. Sano, and G. Mizutani, "Optical second harmonic intensity images of hydrogen deficiency on H-Si(111) surfaces," *e-Journal of Surface Science and Nanotechnology*, vol. 4, pp. 105–109, 2006.

[24] Y. Miyauchi, H. Sano, and G. Mizutani, "Numerical analysis of second harmonic intensity images of a H-Si(111) surface after UV light pulse irradiation," *Applied Surface Science*, vol. 255, no. 5, pp. 3442–3446, 2008.

[25] P. Guyot-Sionnest, "Coherent processes at surfaces: free-induction decay and photon echo of the Si-H stretching vibration for H/Si(111)," *Physical Review Letters*, vol. 66, no. 11, pp. 1489–1492, 1991.

[26] M. Flörsheimer, C. Brillert, and H. Fuchs, "Chemical imaging of interfaces by sum-frequency generation," *Materials Science and Engineering C*, vol. 8-9, pp. 335–341, 1999.

[27] K. Cimatu, H. J. Moore, T. R. Lee, and S. Baldelli, "Sum frequency generation imaging of microcontact-printed monolayers derived from aliphatic dithiocarboxylic acids: contrast based on terminal-group orientation," *Journal of Physical Chemistry C*, vol. 111, no. 32, pp. 11751–11755, 2007.

[28] Y. Miyauchi, H. Sano, J. Okada, H. Yamashita, and G. Mizutani, "Simultaneous optical second harmonic and sum frequency intensity image observation of hydrogen deficiency on a H-Si(111) 1 × 1 surface after IR light pulse irradiation," *Surface Science*, vol. 603, no. 19, pp. 2972–2977, 2009.

[29] K. T. T. Hien, Y. Miyauchi, and G. Mizutani, "Pump-probe time-resolved sum frequency spectroscopy of the H-Si(111)1 × 1 surface," *e-Journal of Surface Science and Nanotechnology*, vol. 8, pp. 89–92, 2010.

[30] G. Mizutani and Y. Miyauchi, "Development and application of optical sum frequency microscopy," *Surface and Interface Analysis*, vol. 42, no. 10-11, pp. 1675–1679, 2010.

[31] Y. Miyauchi, H. Sano, J. Okada, H. Yamashita, and G. Mizutani, "Experimental and numerical analysis of sum frequency microscopic images of a H-Si(111)1 × 1 surface after IR light

pulse irradiation," *Surface and Interface Analysis*, vol. 42, no. 10-11, pp. 1667–1670, 2010.

[32] K. T. T. Hien, Y. Miyauchi, and G. Mizutani, "Construction of a pump-probe system for observing time-resolved sum frequency images," *Surface and Interface Analysis*, vol. 42, no. 10-11, pp. 1671–1674, 2010.

[33] Y. R. Shen and V. Ostroverkhov, "Sum-frequency vibrational spectroscopy on water interfaces: polar orientation of water molecules at interfaces," *Chemical Reviews*, vol. 106, no. 4, pp. 1140–1154, 2006.

[34] B. G. Koehler and S. M. George, "Laser-induced desorption of H2 from Si(111)7 × 7," *Surface Science*, vol. 248, no. 1-2, pp. 158–172, 1991.

[35] E. D. Palik, *Handbook of Optical Constants of Solids*, Academic Press, Boston, Mass, USA, 1985.

[36] R. F. Wood, C. W. White, and R. T. Young, *Semiconductors and Semimetals*, Academic Press, Orlando, Fla, USA, 1984.

[37] R. Gunnella, M. Ali, M. Abbas, F. D'Amico, E. Principi, and A. Di Cicco, "Depth profiling of melting and metallization in Si(111) and Si(001) surfaces," *Physical Review Letters*, vol. 107, no. 16, Article ID 166103, 2011.

[38] G. A. Reider, U. Höfer, and T. F. Heinz, "Desorption kinetics of hydrogen from the Si(111)7 × 7 surface," *The Journal of Chemical Physics*, vol. 94, no. 5, pp. 4080–4083, 1991.

[39] H. Sano, G. Mizutani, W. Wolf, and R. Podloucky, "Ab initio study of linear and nonlinear optical responses of Si(111) surfaces," *Physical Review B*, vol. 66, no. 19, Article ID 195338, 6 pages, 2002.

[40] V. I. Gavrilenko and F. Rebentrost, "Nonlinear optical susceptibility of the (111) and (001) surfaces of silicon," *Applied Physics A*, vol. 60, no. 2, pp. 143–146, 1995.

[41] P. Guyot-Sionnest, "Effect of substrate photoexcitation on the dynamics of the Si-H stretch for Si(111)/H," *Journal of Electron Spectroscopy and Related Phenomena*, vol. 64-65, pp. 1–9, 1993.

[42] M. Rasolt, A. M. Malvezzi, and H. Kurz, "Plasmon-phonon-assisted electron-hole recombination in silicon at high laser fluence," *Applied Physics Letters*, vol. 51, no. 26, pp. 2208–2210, 1987.

[43] Y. D. Glinka, N. H. Tolk, X. Liu, Y. Sasaki, and J. K. Furdyna, "Hot-phonon-assisted absorption at semiconductor heterointerfaces monitored by pump-probe second-harmonic generation," *Physical Review B*, vol. 77, no. 11, Article ID 113310, 2008.

[44] P. Dumas, Y. J. Chabal, and G. S. Higashi, "Coupling of an adsorbate vibration to a substrate surface phonon: H on Si(111)," *Physical Review Letters*, vol. 65, no. 9, pp. 1124–1127, 1990.

[45] M. W. Rowe, H. Liu, G. P. Williams, and R. T. Williams, "Picosecond photoelectron spectroscopy of excited states at Si(111)$\sqrt{3} \times \sqrt{3}R30^\circ$-B, Si(111)7 × 7, Si(100)2 × 1, and laser-annealed Si(111)1 × 1 surfaces," *Physical Review B*, vol. 47, no. 4, pp. 2048–2064, 1993.

[46] A. Bandara, S. Katano, J. Kubota et al., "The effect of co-adsorption of on-top CO on the sum-frequency generation signal of bridge CO on the Ni(111) surface," *Chemical Physics Letters*, vol. 290, no. 1–3, pp. 261–267, 1998.

[47] P. Gupta, V. L. Colvin, and S. M. George, "Hydrogen desorption kinetics from monohydride and dihydride species on silicon surfaces," *Physical Review B*, vol. 37, no. 14, pp. 8234–8243, 1988.

[48] M. L. Wise, B. G. Koehler, P. Gupta, P. A. Coon, and S. M. George, "Comparison of hydrogen desorption kinetics from Si(111)7 × 7 and Si(100)2 × 1," *Surface Science*, vol. 258, no. 1–3, pp. 166–176, 1991.

[49] V. De Renzi, R. Biagi, and U. Del Pennino, "Study of the transition from the ideal Si(111)-H(1×1) surface to the (7×7) reconstruction by HREELS, UPS and LEED," *Surface Science*, vol. 497, no. 1–3, pp. 247–253, 2002.

[50] R. L. Lo, I. S. Hwang, M. S. Ho, and T. T. Tsong, "Diffusion of single hydrogen atoms on Si(111)-(7×7) surfaces," *Physical Review Letters*, vol. 80, no. 25, pp. 5584–5587, 1998.